Advances in Colloid and Interface Science 222 (2015) 148–161

Contents lists available at ScienceDirect

Advances in Colloid and Interface Science

journal homepage: www.elsevier.com/locate/cis

Historical perspective

Shear rheology of mixed protein adsorption layers vs their structure studied by surface force measurements☆

Krassimir D. Danov [a], Peter A. Kralchevsky [a,*], Gergana M. Radulova [a], Elka S. Basheva [a], Simeon D. Stoyanov [b,c], Eddie G. Pelan [b]

[a] Department of Chemical Engineering, Faculty of Chemistry and Pharmacy, Sofia University, 1164 Sofia, Bulgaria
[b] Unilever Research & Development, 3133AT Vlaardingen, The Netherlands
[c] Laboratory of Physical Chemistry and Colloid Science, Wageningen University, 6703HB Wageningen, The Netherlands

ARTICLE INFO

Available online 2 May 2014

Keywords:
Mixed protein adsorption layers
Surface rigidity due to hydrophobins
Surface shear storage and loss moduli
Viscoelastic thixotropic model
Surface shear elasticity and viscosity
Disjoining pressure isotherms

ABSTRACT

The hydrophobins are proteins that form the most rigid adsorption layers at liquid interfaces in comparison with all other investigated proteins. The mixing of hydrophobin HFBII with other conventional proteins is expected to reduce the surface shear elasticity and viscosity, E_{sh} and η_{sh}, proportional to the fraction of the conventional protein. However, the experiments show that the effect of mixing can be rather different depending on the nature of the additive. If the additive is a globular protein, like β-lactoglobulin and ovalbumin, the surface rigidity is preserved, and even enhanced. The experiments with separate foam films indicate that this is due to the formation of a bilayer structure at the air/water interface. The more hydrophobic HFBII forms the upper layer adjacent to the air phase, whereas the conventional globular protein forms the lower layer that faces the water phase. Thus, the elastic network formed by the adsorbed hydrophobin remains intact, and even reinforced by the adjacent layer of globular protein. In contrast, the addition of the disordered protein β-casein leads to softening of the HFBII adsorption layer. Similar (an even stronger) effect is produced by the nonionic surfactant Tween 20. This can be explained with the penetration of the hydrophobic tails of β-casein and Tween 20 between the HFBII molecules at the interface, which breaks the integrity of the hydrophobin interfacial elastic network. The analyzed experimental data for the surface shear rheology of various protein adsorption layers comply with a viscoelastic thixotropic model, which allows one to determine E_{sh} and η_{sh} from the measured storage and loss moduli, G' and G''. The results could contribute for quantitative characterization and deeper understanding of the factors that control the surface rigidity of protein adsorption layers with potential application for the creation of stable foams and emulsions with fine bubbles or droplets.

Contents

☆ This article is dedicated to Dr. habil. Reinhard Miller on the occasion of his 65th birthday.

* Corresponding author. Tel.: +359 2 962 5310; fax: +359 2 962 5643.
E-mail address: pk@lcpe.uni-sofia.bg (P.A. Kralchevsky).

http://dx.doi.org/10.1016/j.cis.2014.04.009
0001-8686/

1. Introduction

Surface dilatational and shear rheology of surfactant and protein adsorption layers at liquid interfaces have been extensively studied in relation to the stability of foams and emulsion [1–8]. Dense adsorption layers that exhibit higher surface elasticity and viscosity can suppress the Ostwald ripening and the coalescence of bubbles or drops [9]. The foams produced from protein solutions are coarse and unstable. However, it was recently established that the protein hydrophobin, which forms very rigid adsorption layers, is an excellent stabilizer of foams with fine bubbles [10,11]. For this reason, the present article is focused on the shear rheology of the viscoelastic adsorption layers from hydrophobin and its mixtures with other proteins and surfactants.

The hydrophobins represent a class of amphiphilic proteins that upon adsorption at the air–water and oil–water interfaces form layers of the highest surface elasticity and viscosity among the investigated proteins [11–16]. The easiest way to visualize their special properties is to shake a hydrophobin aqueous solution, which immediately becomes turbid because of the formation of numerous microscopic bubbles stabilized by this protein. A closer examination of these bubbles indicates that they have irregular (non-spherical) shape [17,18]. The latter is due to the fast solidification of the protein adsorption layer at the bubble surface, which preserves the instantaneous elongated bubble shape acquired in the course of stirring. These properties of hydrophobins make them very efficient stabilizers of foams [11,12,19–21] and emulsions [22–24]. For example, the shaking of water solutions of common milk or egg proteins, like β-lactoglobulin (BLG), β-casein, or ovalbumin (OVA), produces foams with millimeter to centimeter sized bubbles, which decay within 1 min to 1 h [25]. In contrast, the agitation of hydrophobin solutions leads to the formation of foams that remain stable for weeks and months and contain bubbles of average diameter below 100 μm [10,11].

Another valuable property of hydrophobins is that they are rather "sticky" molecules — they can adhere at various surfaces and are used for the immobilization of functional molecules at substrates [26], and as coating agents for surface modification [27,28]. The conventional amphiphilic molecules stabilize foam or emulsion films because their hydrophilic moieties, which are facing the film interior, give rise to a repulsive force between the two film surfaces. In contrast, two adsorption monolayers from hydrophobin HFBII, when brought in close contact, stick to each other and form a self-assembled bilayer (S-bilayer) with a significant energy gain [29]. It turns out that the "hydrophilic" parts of the HFBII molecules are in fact slightly hydrophobic, and they can adhere to each other in aqueous environment. This adhesive force favors the formation of hydrophobin multilayers [30] and the attachment of hydrophobin aggregates to the film surfaces [18,29–31]. In turn, the steric overlap of the adherent aggregates gives rise to repulsion between the film surfaces, which stabilizes the thin liquid films in combination with the contribution from the electrostatic double layer repulsion [18,29].

The hydrophobins are isolated from filamentous fungi. The self-assembled films from these proteins coat fungal structures and mediate their attachment to surfaces [31]. The application of hydrophobins for the stabilization of foams and emulsions in food industry is impeded by the relatively high price of these proteins. However, as demonstrated in the present article, it is possible to replace a considerable part of the hydrophobin with a milk or egg protein (like BLG and OVA) without reducing the surface elasticity and viscosity. The disordered protein β-casein and the nonionic surfactant Tween 20, which are often used in foods, also produce a strong effect (softening) of the hydrophobin adsorption layers. To understand how the differences between the rheological behavior of the investigated systems are related to the structure of the respective mixed protein layers, one can apply experiments with thin foam films, which give information about the film thickness, the presence of trapped protein aggregates, and on the interactions in such films. The obtained results indicate that it is possible to replace up to 90–95% of the hydrophobin with a milk or egg protein without any essential decrease of the surface elasticity and viscosity, and reveal the possible reasons for this result.

As known, the surface *shear elasticity* is the property that makes the difference between rigid and fluid interfacial layers [32] and plays a central role in the rheology of viscoelastic protein adsorption layers. For this reason, in Section 4 special attention is paid on the correct determination of the surface shear elasticity and viscosity E_{sh} and η_{sh} from the measured storage and loss moduli, G' and G''. A viscoelastic thixotropic model is developed, and its application is illustrated for adsorption layers containing hydrophobin. The model could be applied for the interpretation of rheological data for any viscoelastic interfacial layers, and could be extended also to dilatational (not only shear) surface rheology.

2. Experimental methods and systems

2.1. Rotational rheometer

A rotational rheometer, equipped with a biconical tool, is a useful instrument for investigation of interfacial rheology [12,14,15,33]. The working solution is poured up to the edge of the bi-cone (Fig. 1a). The investigated ring-shaped interfacial layer is confined between the outer radius of the bi-cone, R_1, and the inner radius of the cylindrical cell, R_2. The primary data given by the apparatus are the rotational angle γ and the torque τ as functions of time t. The *shear stress* can be calculated from the measured torque by using the formula [33,34]:

$$\tau_{sh} = g_f \tau, \quad g_f \equiv \frac{1}{4\pi}\left(\frac{1}{R_1^2} - \frac{1}{R_2^2}\right) \tag{1}$$

where g_f is a geometrical factor. Eq. (1) is applicable to surface layers of arbitrary viscoelastic behavior in the case of narrow gap, that is for $(R_2 - R_1)/R_1 \le 0.1$.

The *shear strain* is equal to $\tan\gamma$. In the experiments described here, the rotation angle is small so that $\tan\gamma \approx \gamma$. For this reason, hereafter we will use the notation γ for both strain (measured in %) and rotation angle (measured in radians); 1 mrad = 0.1%. Moreover, γ_a denotes the strain amplitude (in oscillatory regime), and $\dot{\gamma}$ denotes the rate of strain, which represents also the angular velocity and the shear rate.

The experimental results reported and discussed in the present article have been obtained with a Bohlin Gemini rheometer (Malvern, UK), using a biconical tool. For this setup, the parameters in Eq. (1) are: $R_1 = 2.81$ cm; $R_2 = 3.0$ cm, and $g_f = 12.36$ rad/m^2.

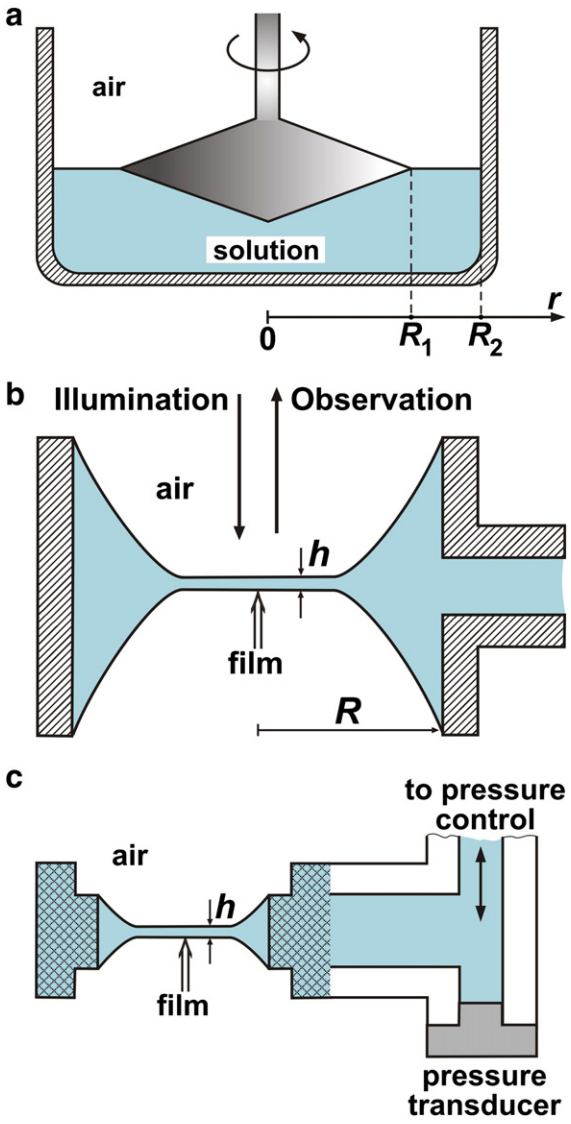

Fig. 1. Sketches of the experimental setups. (a) Rotational rheometer with a biconical tool [33]. (b) Scheludko–Exerowa (SE) cell [35,36], where a foam film of thickness h is formed in a cylindrical capillary of inner radius R. (c) Mysels–Jones (MJ) cell [39], where the foam film is formed in the center of a hole in a porous plate.

Two types of rheological measurements have been carried out. In *fixed-rate-of-strain regime* (angle-ramp regime) the biconical tool rotates with a fixed angular velocity, $\dot{\gamma} \equiv d\gamma/dt$, and the increase of the torque, τ, is recorded as a function of time, t. Six different fixed angular velocities, viz. $\dot{\gamma} = 8.73$, 17.5, 35, 70, 140 and 280 μrad/s, have been used. The maximal value of the rotation angle was $\gamma_b = 14$ mrad. The experiments at fixed rate of strain allow one to determine whether the adsorption layer complies with a rheological model of Kelvin's or Maxwell's type (i.e. parallel or sequential connection of the elastic and viscous elements) [15].

In *oscillatory regime*, the rotation angle oscillates with given amplitude γ_a and frequency ν. The corresponding periodic variations in the torque are registered. Experiments have been carried out at amplitudes $\gamma_a = 1.75$, 5.23, 10.5 and 21.0 mrad and frequencies $\nu = 0.01$, 0.02, 0.05, 0.1, 0.2, 0.5 and 1 Hz. Higher frequencies were not used to avoid disruption of the viscoelastic protein adsorption layer. For example, our experiments [15] showed that the hydrophobin interfacial layer breaks at $\nu = 4$ Hz.

2.2. Scheludko–Exerowa cell

The Scheludko–Exerowa (SE) cell [35,36] was used in the experiments with individual free foam films. The investigated solution is loaded in a cylindrical capillary (of inner radius $R = 1.2$ mm in our experiments) through an orifice in its wall; see Fig. 1b. Thus, a biconcave drop is formed inside the capillary. Next, liquid is sucked through the orifice and the two menisci approach each other until a liquid film is formed in the central part of the cell. By injecting or sucking liquid through the orifice, one can vary the radius of the formed film. Its thickness can be measured by means of an interferometric method [36] of accuracy better than 0.5 nm [37]. For this purpose, the light reflected from the film is supplied to a photomultiplier and computer, and the film thickness is recorded in the course of the experiment. The SE cell is placed in a closed container so that the water vapors are equilibrated with the solution, and evaporation from the film is prevented. The experiments under these conditions are referred as experiments in *closed cell*. If the glass cover of the container is removed, evaporation of water from the film happens. In this case, the film can become considerably thinner. Measurements under these conditions are referred as experiments in *open cell*. A modified version of this cell with two side capillaries, which allow sequential adsorption of two proteins on the film surfaces, was proposed by Wierenga et al. [38].

2.3. Mysels–Jones cell

The Mysels–Jones (MJ) cell [39], known also as thin-film-pressure balance (TFPB) [40,41], allows one to press the two film surfaces against each other at higher pressures (up to 3000 Pa in our experiments). The cylindrical film holder is made of porous glass, so that the solution is supplied in the cell through the pores. In our experiments, the average pore diameter was relatively large, 40 μm, to avoid blocking of pores by protein aggregates. The MJ cell enables one to measure isotherms of the disjoining-pressure Π vs the film thickness h. Experimentally, the applied pressure (which equals Π at equilibrium) is varied and the respective equilibrium value of h is determined form the intensity of light reflected from the film using the interference method [35,36]. A detailed description of the used MJ cell and of the operational procedure can be found elsewhere [42].

2.4. Investigated systems and procedures

At low shear rates, the torque registered by the rotational rheometer is entirely due to the rheological response of the interfacial adsorption layer (rather than to the bulk friction), supposedly the layer has a sufficiently high rheological response. Very appropriate for such studies are the hydrophobins, which form adsorption layers of high surface shear modulus [12]. The dilatational and shear elasticity of hydrophobin HFBII layers has been investigated in Refs. [14–16]. In the present article, our attention is focused on the effect of additives, such as the proteins β-lactoglobulin; ovalbumin, and β-casein, as well as the nonionic surfactant Tween 20.

The class II hydrophobin HFBII was produced via fermentation using the fungus *Trichoderma reesei* [18]. HFBII has molecular weight $M_w = 7.2$ kDa and consists of 70 amino acids with 4 disulfide bonds. Before use, the aqueous HFBII solutions were sonicated in an ultrasonic bath to disperse the formed hydrophobin aggregates. At a concentration of 0.005 wt.% HFBII, the surface tension levels off after 60 s, supposedly, a dense adsorption layer is formed. The adsorption of HFBII at the air/water interface is irreversible and the formed rigid adsorption layers are incompressible, except the case of low surface coverage [16]. Any compression leads to compaction of the HFBII layer, folding, and forcing out of protein, which does not desorb, but forms adjacent "pimples" [30]. Such complications are absent in the experiments considered here, which refer to shearing at constant surface area.

The used globular protein β-lactoglobulin (BLG) from bovine milk has $M_w = 18.4$ kDa; consists of 162 amino acids with 2 disulfide bonds. The used disordered protein β-casein from bovine milk has $M_w = 24$ kDa and consists of 290 amino acids without disulfide bonds. The used globular protein ovalbumin (OVA) from chicken eggs has $M_w = 45$ kDa and consists of 385 amino acids with 1 intrachain disulfide bond. The used nonionic surfactant Tween 20 ($C_{58}H_{114}O_{26}$–polyoxyethylene 20-sorbitan monolaurate) has $M_w = 1228$ kDa. The critical micelle concentration (CMC) of Tween 20 is ≈50 μM [43]. At concentrations below the CMC, Tween 20 is unable to displace the hydrophobin from the interface, as indicated by the rheological data (see below).

In the mixed solutions, all components (HFBII, Tween 20 and the other proteins) were put together in the aqueous phase and sonicated to disperse the formed aggregates before loading in the rheometer. After loading the solution, we waited for 5 min for the formation and consolidation of the protein adsorption layer [14,15,34]. All experiments were performed at a temperature of 25 °C.

Under the used low shear rates, the viscosity of the aqueous subphase did not give any measurable effect. No rheological response was registered also for solutions of conventional surfactants, like Tween 20. For the adsorption layers of OVA, a certain rheological response was registered, whereas for BLG and β-casein this response was much weaker — almost negligible. Well pronounced rheological response was registered only if hydrophobin is present at the air–water interface, i.e. for HFBII solutions and mixed solutions of HFBII with Tween 20, BLG, OVA and β-casein. In other words, the sensitivity of the used rotational rheometer is appropriate for measurements of surface rheology with hydrophobin-containing interfacial layers. The surface rheological response of protein layers from BLG and β-casein (without hydrophobin) can be detected with other more sensitive devices [12].

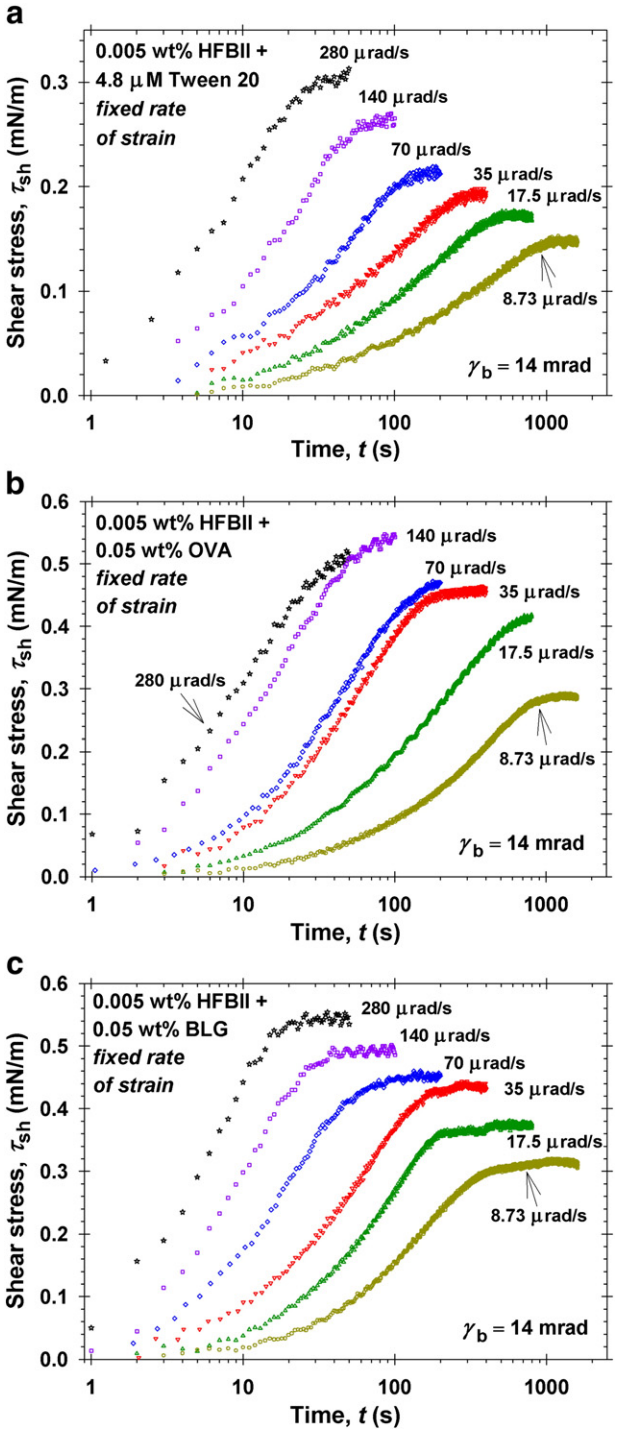

Fig. 2. Plots of the shear stress, τ_{sh}, vs. time, t, at six different fixed angular velocities denoted in the figures. The data are for mixed adsorption layers from 0.005 wt.% HFBII with added: (a) 4.8 μM Tween 20; (b) 0.05 wt.% OVA; (c) 0.05 wt.% BLG. For all curves, the shearing ends at the same rotational angle $\gamma_b = 14$ mrad.

3. Rheological dependences in different dynamic regimes

Here, we present and discuss results obtained in two different dynamic regimes: (i) fixed-rate-of-strain and (ii) oscillatory regime.

3.1. Fixed-rate-of-strain regime

In this regime, the rotational angle γ increases at $\dot{\gamma} = \text{const}$. Fig. 2 shows plots of experimental data for τ_{sh} vs t, at six different shear rates in the range $8.73 \le \dot{\gamma} \le 280$ μrad/s for three different experimental systems: HFBII + Tween 20; HFBII + OVA, and HFBII + BLG. In all runs, the experiment ends at $\gamma = \gamma_b \equiv 14$ mrad. Because of the different $\dot{\gamma}$, the shearing time varies from 50 s for the fastest experiment to 1600 s for the slowest experiment. In Fig. 2, for each of the three investigated systems the shear stress τ_{sh} increases with time, t, and with the rise of shear rate, $\dot{\gamma}$.

Fig. 3a shows plots of experimental data for the shear stress τ_{sh} vs t obtained at the same HFBII concentration (0.005 wt.%) and at the same rate of strain, $\dot{\gamma} = 35$ μrad/s, but at 6 different concentrations of added Tween 20. The data indicate that the rheological response of the system weakens upon the rise of Tween 20 concentration.

The curves in Figs. 2 and 3 are very similar by shape to the analogous rheological curves for HFBII alone and for HFBII + β-casein mixtures [14,15], which comply with the Maxwell's rheological model of a viscoelastic body (see the inset in Fig. 3b):

$$\frac{1}{E_{sh}}\frac{d\tau_{sh}}{dt} + \frac{\tau_{sh}}{\eta_{sh}} = \frac{d\gamma}{dt}. \tag{2}$$

Here, E_{sh} and η_{sh} are, respectively, the surface shear elasticity and viscosity. The integration of Eq. (2), along with the initial condition $\tau_{sh}(t = 0) = 0$, yields:

$$\tau_{sh} = \eta_{sh}\dot{\gamma}\left[1 - \exp\left(-\frac{E_{sh}}{\eta_{sh}}t\right)\right]. \tag{3}$$

All experimental curves in Figs. 2 and 3 are in excellent agreement with the Maxwell model. Eq. (3) fits to the data with a regression coefficients better than 0.9995. Fig. 3b illustrates the agreement between the data and Eq. (3) for experimental curves measured at $\dot{\gamma} = 70$ μrad/s. E_{sh} and η_{sh} are determined from each fit as adjustable parameters. The accuracy of the E_{sh} and η_{sh} values estimated from the fit is very high. For this type of rheological experiment, the accuracy of E_{sh} and η_{sh}

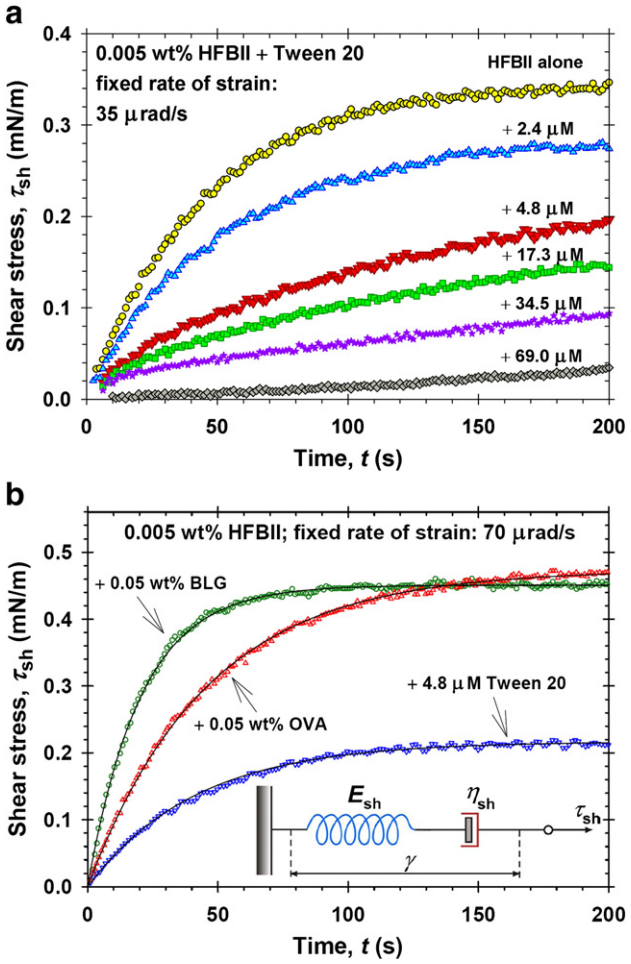

Fig. 3. Plots of experimental data for the shear stress τ_{sh} vs. time t obtained in fixed-rate-of-strain regime at HFBII concentration 0.005 wt.%. (a) Experimental curves obtained at five different concentrations of added Tween 20 at the same shear rate, $\dot{\gamma} = 35$ μrad/s. (b) Fits of typical experimental curves obtained at $\dot{\gamma} = 70$ μrad/s; the solid lines are fits by the Maxwell model (the inset); see Eqs. (2) and (3).

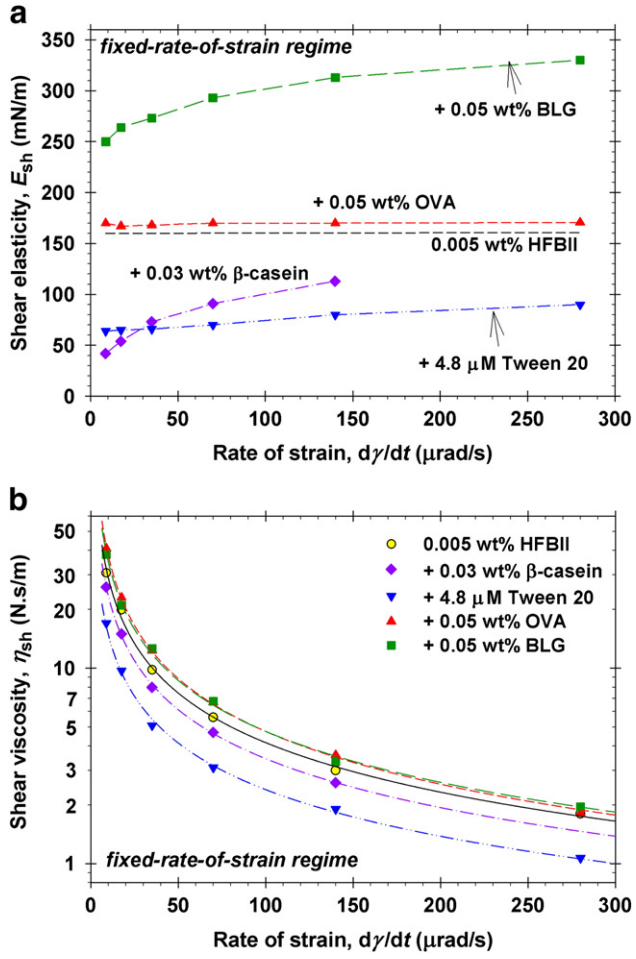

Fig. 4. (a) The shear elasticity, E_{sh}, and (b) the shear viscosity, η_{sh}, plotted vs the rate of strain, $\dot{\gamma}$, at 0.005 wt.% HFBII with and without additives. The lines are guides to the eye.

obtained from a single curve is better than the reproducibility of the experimental curves. The errors of E_{sh} and η_{sh} due to the irreproducibility are 5–10% for E_{sh} and 2–5% for η_{sh}.

For each experimental curve in Figs. 2 and 3, $\dot{\gamma}$ is fixed, so that the values of the shear elasticity and viscosity determined from the fit of such a curve refer to the respective $\dot{\gamma}$, i.e. $E_{sh} = E_{sh}(\dot{\gamma})$ and $\eta_{sh} = \eta_{sh}(\dot{\gamma})$. Fig. 4 shows the plots of E_{sh} and η_{sh} vs $\dot{\gamma}$ obtained from fits of experimental curves. The results for HFBII alone, and for HFBII + β-casein are from Refs. [14,15], whereas the results for HFBII + BLG, OVA, and Tween 20 are those from Fig. 2. The curves in Fig. 4a show that the variation of E_{sh} with $\dot{\gamma}$ is relatively small in the experimental range of $\dot{\gamma}$ values. E_{sh} is either constant or weakly increases. In contrast, η_{sh} strongly decreases with the rise of $\dot{\gamma}$, and for this reason η_{sh} is plotted in log scale in Fig. 4b. For the different systems, the $\eta_{sh}(\dot{\gamma})$ dependencies are similar. The lowest η_{sh} is detected for HFBII + Tween 20.

The most indicative criterion for the degree of solidification of the protein interfacial layer is the value of the surface shear elasticity, E_{sh}. (We recall that $E_{sh} = 0$ for a fluid layer.) From this viewpoint, the most elastic (solidified) adsorption layers are those from HFBII + BLG (Fig. 4a). It seems that these two proteins favorably interact with each other so that their mixing results in a synergistic effect with respect to E_{sh}.

For the HFBII + OVA mixed adsorption layers, E_{sh} is slightly greater than for HFBII alone. In such a case, it is possible to replace a part of HFBII with OVA without decreasing the high elasticity of the adsorption layers, and hopefully, without deteriorating the stability and fine dispersity of the produced foams.

Finally, the addition of β-casein and Tween 20 markedly reduces the elasticity of the HFBII adsorption layers (Fig. 3a). Both β-casein and Tween 20 have hydrophobic chains, which are able to penetrate between the HFBII molecules in the adsorption layer. Most probably, this breaks the elastic network of adherent HFBII molecules and causes the observed decrease of E_{sh} (for more details, see Sections 5.2 and 5.3).

3.2. Oscillatory regime

In oscillatory regime, the variations of the rotational angle γ are sinusoidal,

$$\gamma = \gamma_a \sin(\omega t) \tag{4}$$

where $\gamma_a > 0$ is the amplitude; $\omega = 2\pi\nu$ is the angular frequency and ν is the conventional frequency. The measured shear stress τ_{sh} can be expressed in the form:

$$\frac{\tau_{sh}}{\gamma_a} = G' \sin(\omega t) + G'' \cos(\omega t) \tag{5}$$

where G' and G'' are, respectively, the storage and loss moduli. For a *true linear* response, G' and G'' do not depend on the rate-of-strain amplitude, $\gamma_a\omega$, whereas for a *quasi-linear* response (observed in our experiments) they depend on $\gamma_a\omega$ [15]. The experimental setup allows one to vary γ_a and ω separately. In our previous study on protein adsorption

layers [15] we established that G' and G'' depend on γ_a and ω through their product, $\gamma_a\omega$. Here, this is seen in Fig. 6, where the data correspond to four different γ_a values and seven different ω values.

In the case of linear or quasi-linear response of a viscoelastic body, the plot of τ_{sh} vs. γ (the Lissajous plot) is an ellipse; see Eqs. (4) and (5), and Fig. 5. At all studied amplitudes γ_a and frequencies ν (see Section 2.1), the Lissajous plots are ellipses for the investigated systems. If the viscous contribution to the stress was negligible ($G'' \to 0$), the opening of the ellipse would disappear and it would transform into a segment. The Lissajous plot in Fig. 5 shows that this is not the case, and that the viscous contribution is significant for the investigated systems. The small oscillations around the ellipse in Fig. 5 are due to purely technical reasons — they originate from the electronic feedback built in the used apparatus that preserves the amplitude and frequency of $\gamma(t)$ constant [33].

In the case of *nonlinear* response, Eq. (5) acquires the form of a Fourier expansion that contains sines and cosines of $n\omega t$, where $n = 1, 3, 5, 7, \ldots$. The presence of only odd Fourier modes is related to the fact that the clockwise and anticlockwise rotations are mechanically equivalent (i.e. produce the same elastic and viscous effects) [15,44]. In our present experiments, nonlinear response was observed only at the greater amplitude, $\gamma_a = 2.1\%$, in the case of the HFBII + Tween 20 mixed system. Because the nonlinear response indicates the onset of disruption of the viscoelastic protein layer [15], in the subsequent analysis we take into account only the experimental results that correspond to quasi-linear response, i.e. elliptical Lissajous curves.

Fig. 6 shows experimental data for the storage and loss moduli, G' and G'', as functions of the rate-of-strain amplitude, $\gamma_a\omega$. At the lower values of $\gamma_a\omega$, the effect of the additives on G' is better pronounced. As seen in the figure, the addition of BLG and OVA increases G' with respect to HFBII alone. In contrast, the addition of Tween 20 decreases both G' and G'', i.e. Tween 20 diminishes the rheological response of the HFBII monolayers.

In Fig. 6, at the greater $\gamma_a\omega$ the values of G' become insensitive to the type of additive. In this region, G' decreases and approaches zero at $\gamma_a\omega \approx 0.15\ s^{-1}$, which is an indication for fluidization of the adsorption layer at the larger rate-of-strain amplitudes.

It should be noted that G' and G'' are empirical parameters defined by Eq. (5) and determined directly from the experimental data in oscillatory regime. Characterization of the protein interfacial layer with surface shear elasticity and viscosity, E_{sh} and η_{sh}, is possible only in the framework of an adequate rheological model; see the next section.

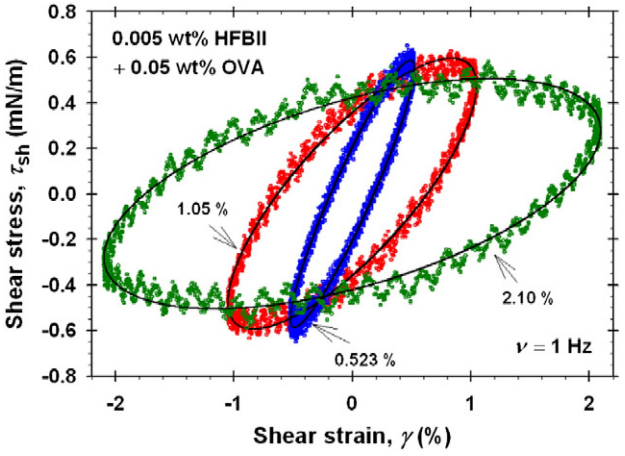

Fig. 5. Lissajous plots of the stress, $\tau_{sh}(t)$, vs the strain, $\gamma(t)$, for 0.005 wt.% HFBII + 0.05 wt.% OVA at frequency $\nu = 1$ Hz and at three different values of the strain amplitude, $\gamma_a = 0.523\%$, 1.05%, and 2.10%.

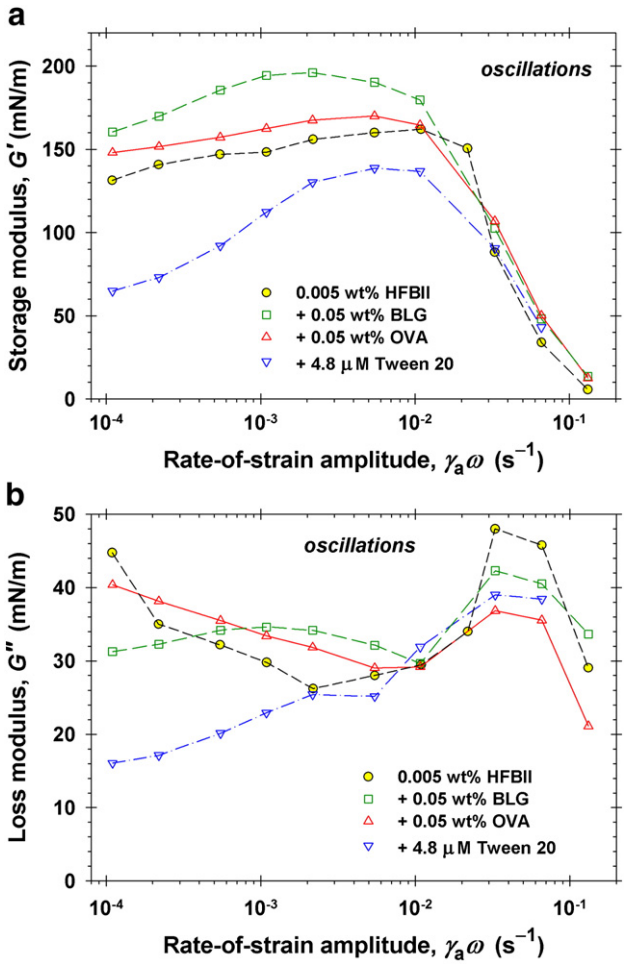

Fig. 6. Plots of the experimentally determined shear moduli vs. the rate-of-strain amplitude, $\gamma_a\omega$, for adsorption layers from 0.005 wt.% HFBII solutions with and without additives: (a) storage modulus G'; (b) loss modulus G''. Each point is the average from six measurements. The dashed lines are guides to the eye.

4. Viscoelastic thixotropic model for interfacial layers

The adequate rheological model can be identified by analysis of a *combined* set of data obtained in fixed-rate-of-strain and oscillatory regimes [15]. Here, the approach developed in Ref. [15] is applied to analyze data for mixed monolayers from HFBII with BLG, OVA and Tween 20.

4.1. Conventional Maxwell model

First, let us consider the conventional Maxwell model with constant E_{sh} and η_{sh}. In this case, substituting $\gamma(t)$ and $\tau_{sh}(t)$ from Eqs. (4) and (5) into Eq. (2), and separating the coefficients before the orthogonal functions $\sin(\omega t)$ and $\cos(\omega t)$, we derive expressions for E_{sh} and η_{sh} in terms of G' and G'':

$$E_{sh} = \frac{G'^2 + G''^2}{G'} \tag{6}$$

$$\eta_{sh} = \frac{G'^2 + G''^2}{G''\omega}. \tag{7}$$

By definition, the *characteristic frequency* ν_{ch} (that equals the reciprocal relaxation time) of the viscoelastic body is:

$$\nu_{ch} \equiv \frac{E_{sh}}{\eta_{sh}} = \frac{G''\omega}{G'} \tag{8}$$

At the last step, we have used Eqs. (6) and (7). In the next section, Eqs. (6), (7) and (8) are generalized to the case of thixotropic layer with variable E_{sh} and η_{sh}.

4.2. Basic equations of the viscoelastic thixotropic model

As illustrated in Fig. 3b, the data obtained at *fixed rate of strain* $\dot{\gamma}$ indicate that the τ_{sh}-vs-t plots obey the Maxwell law, Eq. (3). The values of the shear elasticity and viscosity, E_{sh} and η_{sh}, determined from the fit with the Maxwell law depend on $\dot{\gamma}$; see Fig. 4. As already mentioned, E_{sh} and η_{sh} should be the same irrespective of whether the rotation is clockwise or anticlockwise. For this reason, E_{sh}, η_{sh} and ν_{ch} must depend on the absolute value of $\dot{\gamma}$:

$$E_{sh} = E_{sh}(|\dot{\gamma}|),\ \ \eta_{sh} = \eta_{sh}(|\dot{\gamma}|),\ \ \nu_{ch}(|\dot{\gamma}|) = \frac{E_{sh}}{\eta_{sh}}. \tag{9}$$

Eq. (2) with variable E_{sh} and η_{sh} represents the basic equation of the *viscoelastic thixotropic model* [15] with a single Maxwell element. Acierno et al. [45,46] have considered more general models based on a series of Maxwell elements; see also Section 8.3 in Ref. [47]. It is worthwhile noting that numerous experiments with interfacial layers in Langmuir trough indicate that their viscoelastic behavior complies with the Maxwell model, or its modified versions [48–52].

At fixed rate of strain, the experiments with protein adsorption layers at the air–water interface (rotational rheometer) indicate that the dependence of ν_{ch} on $\dot{\gamma}$ obeys a power law [14,15]:

$$\nu_{ch}(\dot{\gamma}) = Q|\dot{\gamma}|^m. \tag{10}$$

The coefficient Q and the power m are constant parameters of the model. It has been established [14,15] that adsorption layers from HFBII, BLG and β-casein, alone, and by mixed HFBII + β-casein layers obey Eq. (10). Calculating $\nu_{ch} = E_{sh}/\eta_{sh}$ from our data in Fig. 4, we obtain that Eq. (10) is also obeyed for the mixed solutions of HFBII with Tween 20, OVA and BLG; see Fig. 7, where the full symbols correspond to the *fixed-rate-of-strain* regime.

What concerns the *oscillatory* regime, the substitution of $\gamma(t)$ and $\tau_{sh}(t)$ from Eqs. (4) and (5) into Eq. (2) yields:

$$\left(\nu_{ch}G'' + G'\right)\cos(\omega t) + \left(\nu_{ch}G' - G''\right)\sin(\omega t) = E_{sh}\omega\cos(\omega t). \tag{11}$$

Here, in view of Eq. (9) ν_{ch} and E_{sh} depend on t via $\dot{\gamma} = \gamma_a\omega\cos(\omega t)$. The multiplication of Eq. (11) by $\sin(\omega t)$ and $\cos(\omega t)$, with a subsequent integration and some transformations, leads to [15]:

$$\langle\nu_{ch}\rangle \equiv \frac{G''\omega}{G'} = \frac{2}{\pi}\int_0^{\pi}\nu_{ch}(\xi)\sin^2\xi\, d\xi \tag{12}$$

$$\langle E_{sh}\rangle \equiv \frac{2}{\pi}\int_0^{\pi}E_{sh}(\xi)\cos^2\xi\, d\xi = G' + \frac{2G''}{\pi\omega}\int_0^{\pi}\nu_{ch}(\xi)\cos^2\xi\, d\xi \tag{13}$$

where $\xi \equiv \omega t$ is an integration variable; $\langle\nu_{ch}\rangle$ and $\langle E_{sh}\rangle$ are the mean characteristic frequency and the mean surface shear elasticity; see also Eq. (8). If ν_{ch} and E_{sh} are independent of time (of ξ), as in the fixed-rate-of-strain regime, then Eqs. (12) and (13) yield $\langle\nu_{ch}\rangle = \nu_{ch}$ and $\langle E_{sh}\rangle = E_{sh}$ as it should be expected.

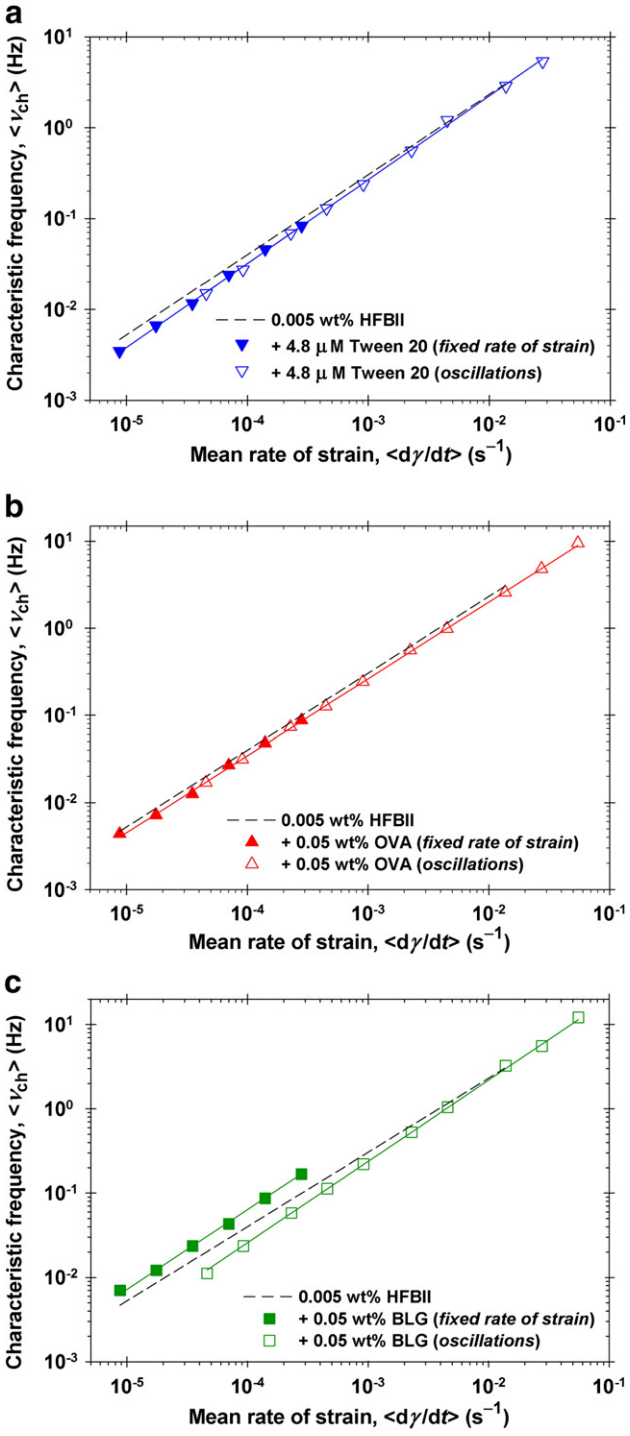

Fig. 7. Plots of the characteristic frequency of rheological response vs the mean rate of strain: (a) 0.005 wt.% + 4.8 μM Tween 20; (b) 0.005 wt.% + 0.05 wt.% OVA; (c) 0.005 wt.% + 0.05 wt.% BLG. For the fixed-rate-of-strain regime, the plot is $\nu_{ch} \equiv E_{sh}/\eta_{sh}$ vs $\dot{\gamma}$. For the oscillatory regime, the respective mean quantities are plotted, $\langle\nu_{ch}\rangle \equiv G''\omega/G'$ vs $\langle\dot{\gamma}\rangle$. The lines represent the best fits by Eqs. (10) and (14).

In the case of oscillatory regime, we substitute $\nu_{ch}(\xi) = Q|\dot{\gamma}|^m$ from Eq. (10) with $\dot{\gamma} = \gamma_a\omega\cos(\xi)$ in the right-hand side of Eq. (12). The integral can be solved and the result can be presented in the form [15]:

$$\langle\nu_{ch}\rangle = Q\langle\dot{\gamma}\rangle^m \tag{14}$$

$$\langle\dot{\gamma}\rangle \equiv \mu\gamma_a\omega,\quad \mu \equiv \left[\frac{\Gamma(m/2+0.5)}{\pi^{1/2}\Gamma(m/2+2)}\right]^{1/m}. \tag{15}$$

Here, $\Gamma(x)$ is the gamma function; Q, m and μ are constant parameters. In analogy with Eq. (10), Eq. (14) expresses the mean characteristic frequency $\langle\nu_{ch}\rangle$ as a power function of the mean shear rate $\langle\dot{\gamma}\rangle$ defined by Eq. (15). The mean surface shear viscosity can be defined as follows [15]:

$$\langle\eta_{sh}\rangle \equiv \frac{\langle E_{sh}\rangle}{\langle\nu_{ch}\rangle}. \tag{16}$$

The combination of the above equations yields [15]:

$$\langle E_{sh}\rangle = \frac{G'^2 + (m+1)G''^2}{G'} \tag{17}$$

$$\langle\eta_{sh}\rangle = \frac{G'^2 + (m+1)G''^2}{G''\omega}. \tag{18}$$

Eq. (17) can be derived by substituting ν_{ch} from Eq. (10) into the last integral in Eq. (13) and transforming the result of integration with the help of Eqs. (12), (14) and (15). Eq. (18) can be derived by substituting $\langle E_{sh}\rangle$ from Eq. (17) and $\langle\nu_{ch}\rangle = G''\omega/G'$ into Eq. (16). Note that for $m = 0$ Eqs. (17) and (18) reduce to the relationships of the conventional Maxwell model, Eqs. (6) and (7). In other words, Eqs. (17) and (18) represent a generalization of Eqs. (6) and (7) for a viscoelastic *thixotropic* body.

Eqs. (17) and (18) allow one to determine the mean surface shear elasticity and viscosity, $\langle E_{sh}\rangle$ and $\langle\eta_{sh}\rangle$, from the values of G' and G'' measured in oscillatory regime. For this goal, $\langle\nu_{ch}\rangle = G''\omega/G'$ is plotted vs $\gamma_a\omega$ in double logarithmic scale, and the power m is determined from the slope of the linear regression (in double-log scale) in accordance with Eqs. (14) and (15); see Fig. 7. With the obtained value of m one calculates $\langle E_{sh}\rangle$ and $\langle\eta_{sh}\rangle$ from Eqs. (17) and (18) substituting the experimental values of ω, G' and G''.

4.3. Test of the model against experimental data

Following the above procedure, from the experimental data for G' and G'' obtained in the oscillatory regime (Fig. 6) we calculated $\langle\nu_{ch}\rangle = G''\omega/G'$ and plotted it vs $\gamma_a\omega$ to determine m. Next, μ was calculated from the determined m using Eq. (15). Furthermore, the values of $\langle\dot{\gamma}\rangle \equiv \mu\gamma_a\omega$ are calculated, and $\langle\nu_{ch}\rangle$ is plotted vs $\langle\dot{\gamma}\rangle$ – see the empty points in Fig. 7. Fig. 7a shows that the data for HFBII + Tween 20 obtained in fixed-rate-of-strain and oscillatory regimes are in excellent agreement and comply with the same straight line in double-log scale, in accordance with Eq. (14). Such agreement between the results in fixed-rate-of-strain and oscillatory regimes has been established for HFBII + OVA (Fig. 7b), HFBII alone and for the HFBII + β-casein mixture in Ref. [15]. From the slope and intercept of the respective linear regression, one can determine the parameters m and Q again, this time from the combined sets of data obtained in the oscillatory and fixed-rate-of-strain regimes.

The determined m and Q, and the respective μ calculated from Eq. (15), are given in Table 1, where they are compared with the values of the same parameters obtained for HFBII alone and for the HFBII + β-casein mixture in Ref. [15]. For the investigated systems, the parameter values in Table 1 are not so different. Most probably, the reason is that in all investigated cases the rheological response of the systems is dominated by the hydrophobin. This is seen also in Fig. 5a (HFBII + Tween 20) and Fig. 7b (HFBII + OVA), where the experimental points for the mixed systems are not so far from the dashed line corresponding to the best fit for HFBII alone.

Table 1
Rheological parameters of viscoelastic adsorption layers determined from fits of experimental data; see Eqs. (14) and (15), and Fig. 7.

Solution	m	Q [s^{m-1}]	μ
0.005 wt.% HFBII[a]	0.88	134	0.413
+0.03 wt.% β-casein[a]	1.18	1538	0.440
+4.8 μM Tween 20	0.92	157	0.417
+0.05 wt.% OVA	0.88	116	0.413
+0.05 wt.% BLG (oscillatory regime)	0.96	187	0.421
+0.05 wt.% BLG (fixed rate of strain)	0.95	395	–

[a] Data from Ref. [15].

The only case in which the double-log plots of data for $\langle\nu_{ch}\rangle$ vs $\langle\dot{\gamma}\rangle$ from the fixed-rate-of-strain and oscillatory regimes do not comply with *the same* straight line is the case of mixed layers from HFBII + BLG – see Fig. 7c. In this case, the data obtained in the two regimes comply with two different straight lines with almost the same slope m, but with different intercepts, Q; see the last two rows of Table 1. In our opinion, this difference is due to the enhancement of the surface rheology caused by BLG, which can be registered during the gentle treatment of the layer at fixed rate of strain. It seems that the long and more intensive agitation of the interfacial layer during the oscillatory measurements partially fluidizes the BLG sub-layer and eliminates the enhancement of surface rheology due to the BLG (see Section 5.1 about the structure of the adsorption layers from HFBII + BLG).

4.4. Surface shear elasticity and viscosity vs the rate of strain

As described above, in *fixed-rate-of-strain* regime we directly obtain the dependencies $E_{sh}(\dot{\gamma})$ and $\eta_{sh}(\dot{\gamma})$; see Fig. 4 and the related text. In contrast, the *oscillatory* regime gives the dependence of the mean shear elasticity and viscosity, $\langle E_{sh}\rangle$ and $\langle\eta_{sh}\rangle$, on the rate-of-strain amplitude, $\gamma_a\omega$; see e.g. Fig. 8a. To obtain the curves in Fig. 8a, the values of G' and G'' (from Fig. 6) have been substituted in Eqs. (17) and (18), together with the respective values of m from Table 1. As seen in Fig. 8a, the values of $\langle E_{sh}\rangle$ are the greatest for HFBII + BLG, intermediate for HFBII + OVA, and the lowest for HFBII + Tween 20.

Our next task is to obtain the $E_{sh}(\dot{\gamma})$ and $\eta_{sh}(\dot{\gamma})$ dependencies from the data in *oscillatory* regime, and to compare them with the respective dependencies in *fixed-rate-of-strain* regime. For this goal, following Ref. [15] we seek $E_{sh}(\dot{\gamma})$ in the form of an empirical expression:

$$E_{sh}(\dot{\gamma}) = E_1\exp(-t_1|\dot{\gamma}|) + E_2\exp(-t_1|\dot{\gamma}|)[1-\exp(-t_2|\dot{\gamma}|)] \tag{19}$$

where E_1, E_2, t_1 and t_2 are constant parameters. First, using them as adjustable parameters, Eq. (19) can be fitted to the data for $E_{sh}(\dot{\gamma})$ in Fig. 4a. Second, Eq. (19) with $\dot{\gamma} = \gamma_a\omega\sin\xi$ yields the dependence $E_{sh}(\xi)$ under the first integral in Eq. (13), which allows one to determine E_1, E_2, t_1 and t_2 as adjustable parameters from the fits of the dependences of $\langle E_{sh}\rangle$ on $\gamma_a\omega$ in Fig. 8a.

We combined the two fits and determined E_1, E_2, t_1 and t_2 in Eq. (19) as adjustable parameters by fitting *simultaneously* the data obtained in fixed-rate-of-strain (Fig. 4a) and oscillatory (Fig. 8a) regimes. The parameter values obtained in this way are given in Table 2. The best fits are presented with the continuous lines in Fig. 8b, where the points are the data for E_{sh} vs. $\dot{\gamma}$ in fixed-rate-of-strain regime from Fig. 4. The best fits are presented also with the dashed lines in Fig. 8a, in terms of $\langle E_{sh}\rangle$ vs. $\gamma_a\omega$ for the data obtained in the oscillatory regime. The excellent agreement between the theoretical curves and the data points in Fig. 8a and b demonstrates that with the same model (with the same values of the parameters in Tables 1 and 2) one can describe the rheological behavior of the viscoelastic layer in two quite different dynamic regimes: oscillatory and fixed rate-of-strain. In the special case of HFBII + BLG (the upper curve in Fig. 8a), the fit with Eq. (19) was applied only to the data obtained in oscillatory regime; see the discussion related to Fig. 7c above.

The solid lines in Fig. 8c are calculated from the expression $\eta_{sh}(\dot{\gamma}) = E_{sh}(\dot{\gamma})/\nu_{ch}(\dot{\gamma})$, where $E_{sh}(\dot{\gamma})$ is given by Eq. (19) with E_1, E_2, t_1 and t_2 from Table 2, and $\nu_{ch}(\dot{\gamma})$ – by Eq. (10) with Q and m from Table 1.

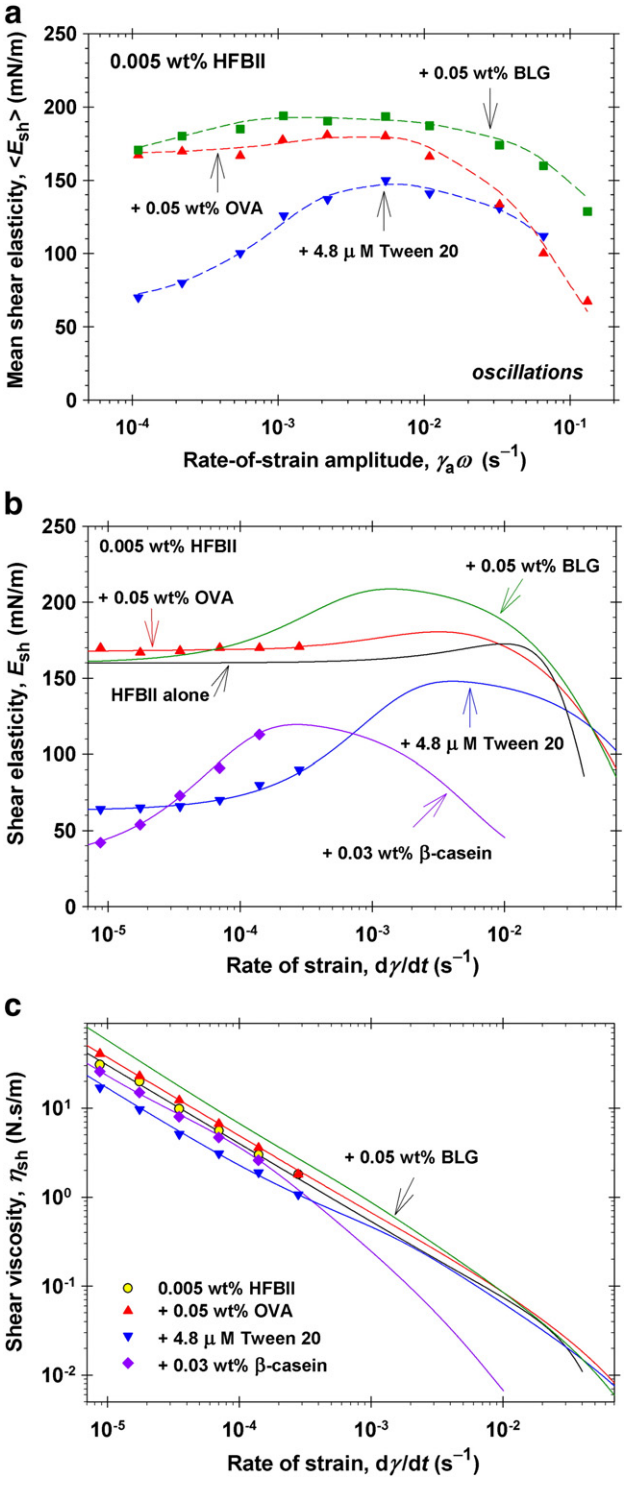

Fig. 8. (a) Plots of $\langle E_{sh}\rangle$ vs. the rate-of-strain amplitude, $\gamma_a\omega$. (b) Plot of the dependence $E_{sh}(\dot{\gamma})$ calculated using Eq. (19) and analogous expressions in Ref. [15]; the points are from Fig. 4a. (c) Plot of the dependence $\eta_{sh}(\dot{\gamma}) = E_{sh}(\dot{\gamma})/\nu_{ch}(\dot{\gamma})$ calculated using Eq. (10) with parameter values from Table 1; the points are from Fig. 4b.

Table 2
Parameters in Eq. (19) determined from fits of data for mixed solutions containing 0.005 wt.% HFBII.

System	E_1 [mN/m]	E_2 [mN/m]	t_1 [s]	t_2 [s]
+4.8 μM Tween 20	63.2	88.9	5.66	1189
+0.05 wt.% OVA	168	22.2	10.6	608
+0.05 wt.% BLG	160	53.4	13.1	2926

For HFBII alone and HFBII + β-casein, the respective expressions and parameter values have been determined in Ref. [5]. The symbols represent the data from Fig. 4b for η_{sh} vs $\dot{\gamma}$ obtained at fixed rate of strain. Again, there is an excellent agreement between the experimental points and the calculated curves.

The comparison of the curves for the different systems in Fig. 8b,c indicates that the addition of BLG and OVA increases both E_{sh} and η_{sh}, whereas the addition of Tween 20 and β-casein decreases both E_{sh} and η_{sh}. However, for the mixed systems their ratio $\nu_{ch} = E_{sh}/\eta_{sh}$ remains close to that of HFBII alone; see Fig. 7. As mentioned above, the main parameter that indicates solidification of the adsorption layer is E_{sh}, rather than ν_{ch}. As seen in Fig. 8a and b, initially E_{sh} increases with the shear rate, but at higher $\dot{\gamma}$ the shear elasticity decreases.

Because the shear deformation occurs at *fixed* surface area, in a compact adsorption layer the breakage of the contact between two neighboring molecules is followed by the establishment of contacts with new neighboring molecules. In this way, the shearing is accompanied with the breakage and formation of intermolecular (inter-protein) bonds. Most probably, the increasing branch of E_{sh} at the lower $\dot{\gamma}$ corresponds to predominant bond formation, whereas the decreasing branch at the higher $\dot{\gamma}$ — to predominant bond breakage.

4.5. Special behavior of the mixed layers from hydrophobin + β-lactoglobulin

For this system, the greatest enhancement of the surface rheology is observed. As seen in Fig. 8a,b, in *oscillatory* regime the maximal values of $\langle E_{sh}\rangle$ and $E_{sh}(\dot{\gamma})$ are approaching 200 mN/m for the HFBII + BLG mixed solutions. At a *fixed rate of strain*, the weakly disturbed HFBII + BLG layer rests in another state of higher elasticity — the maximal value of E_{sh} is about 330 mN/m in Fig. 4a. Among all investigated systems, the HFBII + BLG mixture is the only one, for which the states of the monolayer in fixed-rate-of-strain and oscillatory regimes correspond to two different viscoelastic bodies, as indicated by the difference between the respective lines in Fig. 7c. For this reason, the E_{sh} data for HFBII + BLG in Fig. 4a (fixed rate of strain) cannot be fitted together with the respective data for $\langle E_{sh}\rangle$ in Fig. 8a. For the same reason, the E_{sh} vs $\dot{\gamma}$ curve for HFBII + BLG in Fig. 8b, representing the fit of the data in oscillatory regime, is not expected to comply (and it does not comply) with the respective experimental points at fixed rate of strain in Fig. 4a.

The experimental results for the HFBII + BLG mixture presented above were obtained at a weight ratio 10:1 in favor of BLG, i.e. at $x_{BLG} = 0.91$ weight fraction of BLG in the mixture with HFBII. To clarify what is the effect of x_{BLG} on the values of E_{sh} and η_{sh}, we carried out a series of rheological experiments at various compositions of the protein

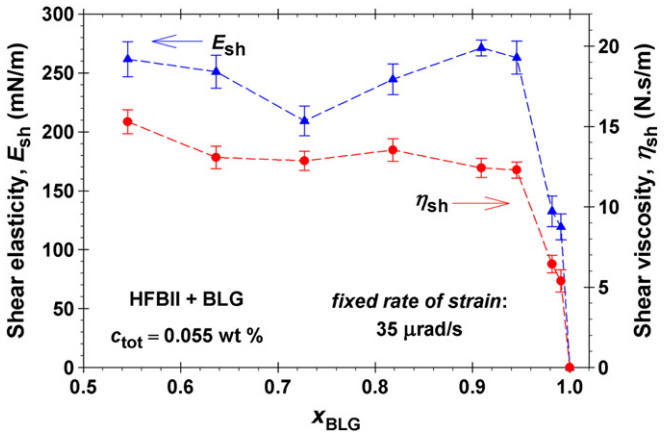

Fig. 9. Shear elasticity, E_{sh}, and viscosity, η_{sh}, of mixed adsorption layers plotted vs. the weight fraction of BLG, x_{BLG}, at a fixed total HFBII + BLG concentration, $c_{tot} = 0.055$ wt.%. E_{sh} and η_{sh} are measured in fixed-rate-of-strain regime at angular velocity $\dot{\gamma} = 35$ μrad/s.

mixture in the range $0.5 \le x_{BLG} \le 1$ at a fixed total protein concentration of 0.055 wt.%. The results are shown in Fig. 9.

Because at $x_{BLG} = 1$, our rotational rheometer registers no rheological response (E_{sh} and η_{sh} are rather low for a layer from BLG alone), we expected that in an intermediate value of x_{BLG} there should be a transition from a state of viscoelastic layer with high E_{sh} and η_{sh} values to a state with zero (undetectably low) values of these parameters. The data in Fig. 7 show that this transition exists and occurs at $x_{BLG} \approx 0.95$. In other words, we can replace up to 95% of HFBII with BLG without reducing the elasticity and viscosity of the mixed interfacial adsorption layer.

From a structural viewpoint, at $0 < x_{BLG} < 0.95$ the more surface active HFBII occupies the air/water interface and forms a rigid adsorption layer, whereas BLG forms a second adsorption layer below the hydrophobin layer, as indicated by the experiments with thin foam films (see the next section). In contrast, at $0.95 < x_{BLG} < 1$ the concentration of HFBII is too low so that the hydrophobin cannot cover the interface with a dense solidifying layer. In this case, a mixed adsorption layer of BLG + HFBII is formed, which leads to a significant decrease in both E_{sh} and η_{sh}, as seen in Fig. 9.

5. Surface forces vs rheological behavior of protein adsorption layers

The experiments with thin liquid films give direct information for the surface forces acting in the films and for the possible structure of the adsorption layers. We performed experiments by the SE and MJ cells. Illustrative results are shown in Figs. 10 and 11. The most probable film structures derived by analysis of the obtained data are sketched in Fig. 12. Details are following.

5.1. Mixed solutions of hydrophobin and globular proteins

The foam films from 0.05 wt.% BLG are relatively thick and stable (Fig. 10a). The addition of 0.005 wt.% HFBII leads to the appearance of aggregates, which are initially trapped in the film (Fig. 10b). At a higher applied pressure, a black film of thickness $h = 17$ nm appears in the middle of the film and gradually expands (Fig. 10c). Eventually, a sudden transition to a 6 nm thick bilayer (S-bilayer) occurs, which is typical for the films from HFBII alone [18,29]. The structure of the S-bilayer is illustrated in Fig. 12d. The S-bilayer spontaneously and considerably expands and occupies a much larger area than the film in its preceding states. Thus, the photograph in Fig. 10d, taken with the same magnification as the other photos in Fig. 10, shows only a small portion of the S-bilayer (the upper-left part of the photo).

Fig. 11a shows experimental dependences of the disjoining pressure Π on the film thickness h obtained by the MJ cell for foam films formed from solutions of 0.005 wt.% HFBII + 0.05 wt.% BLG at two ionic strengths: $I = 1.5$ mM (due to NaN_3), and $I = 11.5$ mM (due to 1.5 mM NaN_3 + 10 mM NaCl). Branch A of the experimental curves, which is registered at the greater thicknesses, can be explained with a superposition of steric and electrostatic interactions due to charged protein aggregates that are attached (adherent) to the film surfaces. Similar branches of the $\Pi(h)$ isotherm have been registered and discussed in Ref. [29]. The presence of electrostatic contribution to the registered $\Pi(h)$ isotherms is evidenced by the decrease of the barriers to the A → B and B → C transition upon the addition of 10 mM NaCl: compare the lower and upper $\Pi(h)$ dependencies in Fig. 11a. Branch C at $h \approx 6$ nm corresponds to an S-bilayer. The S-bilayer can be easily recognized by its thickness equal to the diameters to two HFBII molecules and by the fact that the film area suddenly and significantly increases upon its appearance due to the considerable energy gain that accompanies the adhesion of the two hydrophobin monolayers [29].

The appearance of S-bilayer means that only two HFBII monolayers remain in the film at the end of film thinning. In other words, during the B → C transition (Fig. 11a) the whole amount of BLG has been squeezed out of the film. Thus, we could expect that branch B corresponds to the two-layer film structure depicted in Fig. 12a. The outer layer is that of the more hydrophobic HFBII, which completely occupies the air–water interface. The BLG molecules form a second (inner) layer, which is adherent to the HFBII layer. Probably, the BLG molecules are attached to the interfacial hydrophobin layer at the openings of their hydrophobic pockets [53] as sketched in Fig. 12a. The squeezing of BLG from the film during the B → C transition (Fig. 11a) can be interpreted as a transition from the configuration in Fig. 12a to that in Fig. 12d.

The results for foam films from HFBII + OVA solutions are completely analogous to that for the films from HFBII + BLG solutions. In particular, in both cases at the last step we have a transition from a film of thickness $h \approx 14$ nm (Fig. 12a) to an S-bilayer of uniform thickness $h \approx 6$ nm (Fig. 12d). The formation of S-bilayer is a specific property of HFBII [29]. Such strong adhesion of the adsorption layers on the two film surfaces is not observed with monolayers from BLG or OVA.

The data from the foam film experiments indicate the formation of a two-layered protein structure at the film surfaces: outer layer from HFBII and inner layer from the *globular* protein (BLG or OVA). This interfacial structure correlates with the fact that the addition of BLG or OVA leads to the increase of both E_{sh} and η_{sh} in comparison with HFBII alone; see Figs. 4 and 8. As already mentioned E_{sh} and η_{sh} are rather low ($\tau_{sh} \approx 0$) for adsorption layers from BLG and OVA alone. Hence, the rheological effects from the adjacent HFBII and BLG layers in Fig. 12a are not simply additive (otherwise, we would not register a rise of E_{sh} due to BLG). The enhancement of the surface rheology is probably due to the linking of adsorbed HFBII molecules by adherent BLG (or OVA) molecules. The binding energy between HFBII and BLG must be smaller than the adsorption energy of HFBII at the air–water interface. Otherwise, HFBII would be incorporated in joint aggregates with the BLG in the bulk, and we would not register the presence of dense hydrophobin adsorption layers in our rheological and thin-film experiments.

The aggregation of BLG in the bulk is mostly due to the patch-charge attraction [54], i.e. to the interaction between positively and negatively charged patches on the surface of the BLG molecule [55]. As indicated by

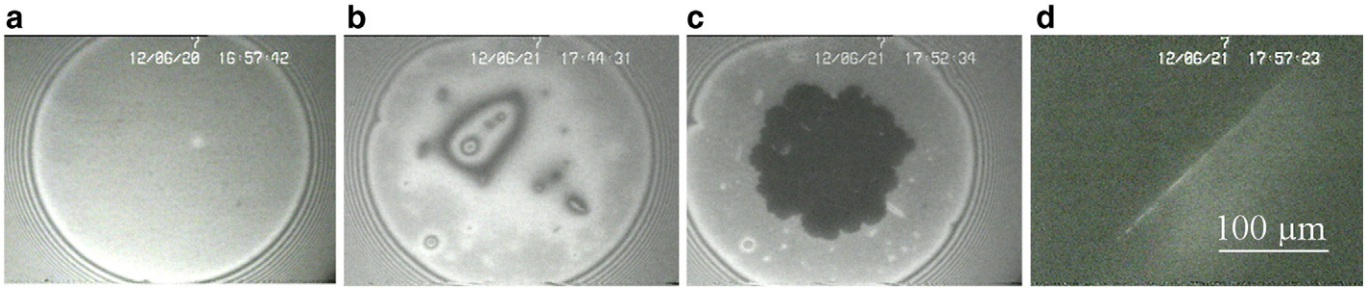

Fig. 10. Photos of foam films in SE cell. (a) Equilibrium film from a solution of 0.05 wt.% BLG; thickness $h = 57$ nm in closed cell. Films from solutions of 0.05 wt.% BLG + 0.005 wt.% HFBII: (b) Thick film with aggregates in closed cell; (c) Appearance of a dark spot of thickness $h = 17$ nm in open cell, followed by (d) the appearance and expansion of an S-bilayer of thickness $h = 6$ nm. The solutions contain 1.5 mM NaN_3. The reference bar of 100 μm is the same for all photos.

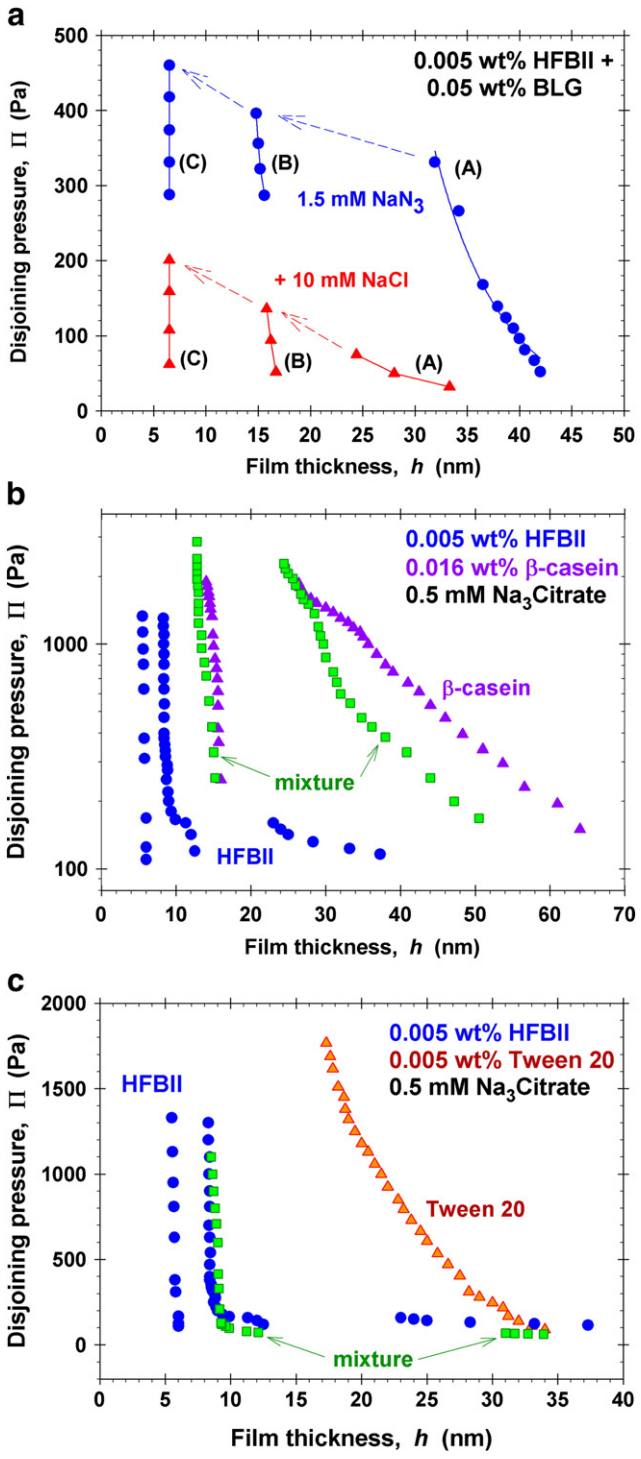

Fig. 11. Disjoining pressure, Π vs. h, isotherms measured by MJ cell. (a) 0.005 wt.% HFBII + 0.05 wt.% BLG with electrolytes. (b) 0.005 wt.% HFBII, 0.016 wt.% β-casein and their mixture. (c) 0.005 wt.% HFBII, 0.005 wt.% Tween 20 and their mixture.

our rheological measurements, the patch–charge interactions do not lead to high E_{sh} and η_{sh} for the BLG adsorption layers, as this happens with the HFBII adsorption layers, which are compacted by hydrophobic interactions [29].

The sketches in Fig. 12 are idealized — except the S-bilayer, which is rather uniform, the HFBII layers may contain voids and adherent hydrophobin aggregates [18,30,31]. From this viewpoint, all rheological properties, such as G', G'', E_{sh} and η_{sh}, represent averaged macroscopic characteristics of the interfacial layer.

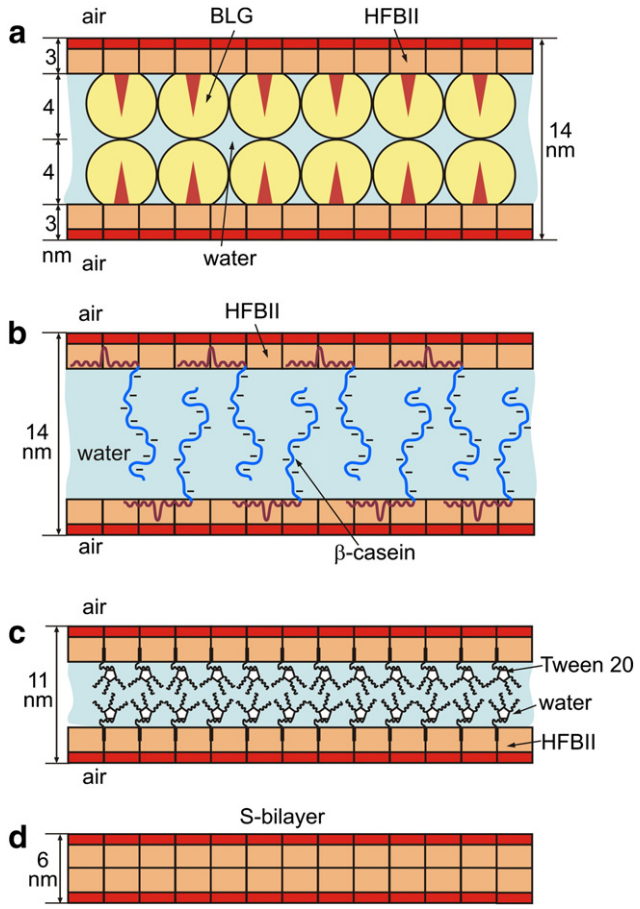

Fig. 12. Sketches of foam films stabilized with HFBII + additives: (a) HFBII + BLG; the sharp cones in the BLG molecules symbolize the hydrophobic pockets of BLG that are expected to contact with the hydrophobin. (b) HFBII + β-casein; (c) HFBII + Tween 20, and (d) S-bilayer from HFBII molecules obtained as a final stage of film thinning.

5.2. Mixed solutions of hydrophobin and a disordered protein

Here, we consider and discuss experimental Π(h) dependences for foam films formed from mixed solutions of HFBII with the disordered protein β-casein in the presence of 0.5 mM Na_3Citrate. Na_3Citrate was used because it lowers the electrostatic barrier to the S-bilayer formation [18,29].

At concentrations 0.005 wt.% HFBII + 0.005 wt.% β-casein, the experimental Π(h) dependences look similar to those in Fig. 11a, with S-bilayer formation at the final stage. However, at concentration 0.005 wt.% HFBII + 0.016 wt.% β-casein (Fig. 11b), the final film from the mixed solution has a thickness in the range $12.8 < h < 15.2$ nm (depending on the applied pressure) and no transition to S-bilayer has been observed even at the highest applied pressure, Π = 2860 Pa. This result indicates that the β-casein molecules are built in the HFBII monolayer and they cannot be forced out of the film as this happens with the BLG or OVA molecules (see above). The situation is similar at the higher concentration of 0.03 wt.% β-casein, which has been used in our rheological experiments (Fig. 8b and c).

Fig. 11b compares the Π(h) dependencies measured with the mixed system with those measured with films formed from solutions of the single proteins: 0.005 wt.% HFBII and 0.016 wt.% β-casein, separately, all of them containing 0.5 mM Na_3Citrate. The right-hand side branches (at $24 < h < 64$ nm) can be explained with the combined electrostatic and steric effects due to the sandwiching of charged protein aggregated within the film, in analogy with branch A in Fig. 11a. The intermediate branches (at $12 < h < 16$ nm) are close for β-casein and for the mixed

system, which indicates that the hydrophobic part of the β-casein molecule is imbedded into the hydrophobin monolayer, whereas the negatively charged part of the β-casein chain is protruding from the interface and provides the combined steric-overlap and electrostatic repulsion that stabilizes these films, as sketched in Fig. 12b.

The β-casein molecule consists of a shorter hydrophilic part (≈20%) and a longer hydrophobic part (≈80%), 290 amino acids in total. The hydrophilic chain includes the amino-acids at position from 1 to 43 at the N-terminus. This chain has 21 negative charges and 5 positive charges so that its net charge is −16 [56]. If the length per amino acid residue is 0.3 nm [57], then the length of the extended hydrophilic chain of β-casein is about 13 nm. However, in water this chain forms an undulated tail of shorter end-to-end distance.

The remaining 80% of the β-casein molecule is very hydrophobic; its net charge is either +1 or +2, depending on the pH. The water is a poor solvent for this chain, so that the β-casein forms micelles of diameter ≈ 13 nm in aqueous solutions [58]. Upon adsorption at the air/water interface, the hydrophobic chain of the β-casein molecule forms trains and loops, whereas the charged hydrophilic part protrudes as a tail in the water phase [59–61]. The same could happen if the hydrophobic part of the β-casein molecule is imbedded into the HFBII adsorption layer (Fig. 11b). As already mentioned, the thickness of the thinnest films with β-casein and with the mixed system, in the range $12 < h < 16$ nm (Fig. 11b), can be explained with the combination of the steric-overlap and electrostatic repulsion, which is due to the protruding hydrophilic parts of the β-casein molecules; see Fig. 12b.

For the surface shear rheology, it is important that the hydrophobic chain of the β-casein molecule is embedded in the HFBII adsorption layer. Note that this hydrophobic chain is about 3.5 times bigger (by number of amino acid residues) than the whole HFBII molecule. At this situation, we could expect that the incorporation of β-casein in the HFBII surface layers should strongly affect their rheology. In our experiments, this has been observed as an essential reduction of both the surface shear elasticity E_{sh} and viscosity η_{sh} — see Figs. 4 and 8. In other words, the addition of β-casein decreases the rigidity of the hydrophobin adsorption layers because of the penetration of the β-casein long hydrophobic chains between the adsorbed HFBII molecules (Fig. 12b) and breakage of their adhesive contacts.

5.3. Mixed solutions of hydrophobin and Tween 20

The experiments with MJ cell show that in the absence of HFBII, for 0.005 wt.% Tween 20 alone, the $\Pi(h)$ dependence corresponds to electrostatic repulsion screened by the added electrolyte; see the rightmost curve in Fig. 11c. Such repulsion is often observed with nonionic surfactants. It has been attributed to the attachment of OH^- ions to the air–water interface between the surfactant headgroups [62].

At a concentration of 0.0008 wt.% (6.5 μM) Tween 20, added to a 0.005 wt.% HFBII solution, the Tween 20 almost completely suppresses the appearance of the intermediate branch of the $\Pi(h)$ isotherm for HFBII alone (that at $h = 9$–10 nm for HFBII in Fig. 11b,c). This could be due to a partial hydrophilization of the lower surface of HFBII monolayer by adsorbed Tween 20 molecules, which prevents the attachment of HFBII aggregates (oligomers) that give rise to the appearance of the considered $\Pi(h)$ branch [29].

At a higher concentration of 0.005 wt.% (40.7 μM) of added Tween 20, S-bilayer of thickness $h \approx 6$ nm is not observed at all, even at the highest attained pressure, $\Pi = 1100$ Pa (Fig. 11c). Instead, the thickness of the final film varies in the range $8.5 \le h \le 12.1$ nm, depending on the applied pressure. This result indicates that the Tween 20 molecules are firmly attached to the HFBII monolayer (Fig. 12c) and they cannot be forced out of the film as this happens with the BLG and OVA molecules (see above). The thickness of the respective films can be explained with the steric-overlap repulsion between the hydrophilic chains of the Tween 20 headgroups.

As in the case of β-casein, the penetration of the hydrophobic chains of the Tween 20 molecules between the HFBII molecules (Fig. 12c) decreases the rigidity of the hydrophobin adsorption layers. This is evidenced by the pronounced decrease in both surface shear elasticity E_{sh} and viscosity η_{sh} for the adsorption layers from mixed HFBII + Tween 20 solutions — see Figs. 4 and 8. The decreasing of the viscoelastic response of the HFBII adsorption layers upon the increase of the concentration of added Tween 20 is also visible in Fig. 3a.

6. Conclusions

The hydrophobins form the most rigid adsorption layers at the air/water interface in comparison with all other investigated proteins. Consequently, one could expect that the mixing of hydrophobin with another conventional protein should lead to a reduction of the surface shear elasticity and viscosity, E_{sh} and η_{sh}, proportional to the fraction of the conventional protein. However, the experiments show that the effect of mixing can be rather different depending on the nature of the additive.

If the additive is a *globular* protein, like BLG and OVA, the surface rheological response of the mixed adsorption layers remains high up to 95 wt.% of the additive in the mixed solutions with HFBII. The experiments with separate foam films indicate that this is due to the formation of a bilayer structure at the air/water interface, viz. the more hydrophobic HFBII forms the upper layer that is adjacent to the air phase, whereas the conventional globular protein (BLG, OVA) forms a second adsorption layer, which is adherent to the hydrophobin layer and faces the water phase (Fig. 12a). Thus, the elastic network formed by the adsorbed hydrophobin remains *intact*, and even reinforced by the adjacent layer of globular protein. This structure of the adsorption layer allows one to replace up to 95 wt.% of hydrophobin in the solution with a conventional globular protein without reducing the surface elasticity and viscosity. At fraction > 95 wt.% of the conventional protein in the bulk, the surface elasticity and viscosity steeply decrease, which can be explained with the penetration of conventional protein in the HFBII adsorption layer and breakage of the elastic hydrophobin network.

If the additive is the *disordered* protein β-casein, it leads to softening of the mixed adsorption layer at fractions comparable or higher than those of HFBII. Similar (an even stronger) effect is produced by the nonionic surfactant Tween 20. This can be explained with the penetration of the hydrophobic tails of β-casein and Tween 20 between the HFBII molecules at the interface (see Fig. 12b and c), which breaks the integrity of the hydrophobin interfacial elastic network.

To quantify the effect of proteins and additives on the shear rheology of viscoelastic adsorption layers one has to determine the surface shear elasticity and viscosity, E_{sh} and η_{sh}. This is a nontrivial task, because the experiment (oscillatory regime) yields the surface storage and loss moduli, G' and G'', which are empirical parameters. The surface elasticity and viscosity, E_{sh} and η_{sh}, can be determined only in the framework of an *adequate* rheological model. The experimental data obtained in (at least) two different dynamic regimes must comply with *the same* model, if it is adequate. This can serve as a criterion for determining the correct model.

For the investigated viscoelastic layers, appropriate are the regimes of (i) fixed rate-of-strain and (ii) oscillations, realized with a rotational rheometer. The *viscoelastic thixotropic model* described in Section 4, which is based on Eqs. (2) and (10), turns out to be the adequate rheological model. The criterion for the applicability of this model is the linearization of the experimental data when plotting the characteristic frequency, $\nu_{ch} \equiv E_{sh}/\eta_{sh}$, vs. the rate of strain, $\dot{\gamma}$, in double log scale; see Eq. (10) and Fig. 7. This criterion is satisfied for all investigated adsorption layers. Moreover, for most proteins (HFBII, BLG, and β-casein alone, and for the mixtures HFBII + OVA and HFBII + Tween 20), the data from the fixed-rate-of-strain and oscillatory regimes comply with *the same* straight line; see e.g. Fig. 7a and b. Only the data for HFBII + BLG complies with two different, but close lines (Fig. 7c),

which could be explained with a partial fluidization of the respective mixed layer in oscillatory regime. The model provides simple expressions, Eqs. (17) and (18), for calculating E_{sh} and η_{sh} from the measured moduli G' and G''.

The results presented and discussed in this article could contribute for the quantitative characterization and deeper understanding of the factors that control the surface rigidity of protein adsorption layers with potential application for the creation of stable foams and emulsions with fine bubbles or droplets.

Acknowledgments

The authors gratefully acknowledge the support from Unilever Research (VL-2011-0698); from the FP7 project Beyond-Everest, and from COST Action CM1101. The authors thank Ms. Mariana Paraskova for her assistance in figure preparation.

References

[1] Miller R, Wüstneck R, Krägel J, Kretzschmar G. Dilational and shear rheology of adsorption layers at liquid interfaces. Colloids Surf A 1996;111:75–118.
[2] Murray BS, Dickinson E. Interfacial rheology and the dynamic properties of adsorbed films of food proteins and surfactants. Food Sci Technol 1996;2:131–45.
[3] Vollhardt D, Fainerman VB. Progress in characterization of Langmuir monolayers by consideration of compressibility. Adv Colloid Interface Sci 2006;127:83–97.
[4] Krägel J, Derkatch SR, Miller R. Interfacial shear rheology of protein-surfactant layers. Adv Colloid Interface Sci 2008;144:38–53.
[5] Miller R, Ferri JK, Javadi A, Krägel J, Mucic N, Wüstneck R. Rheology of interfacial layers. Colloid Polym Sci 2010;288:937–50.
[6] Dan A, Gochev G, Krägel J, Aksenenko EV, Fainerman VB, Miller R. Interfacial rheology of mixed layers of food proteins and surfactants. Curr Opin Colloid Interface Sci 2013;18:302–10.
[7] Mikhailovskaya AA, Noskov BA, Nikitin EA, Lin S-Y, Loglio G, Miller R. Dilational surface viscoelasticity of protein solutions. Impact of urea. Food Hydrocoll 2014;34:98–103.
[8] Mendoza AJ, Guzmán E, Martínez-Pedrero F, Ritacco H, Rubio RG, Ortega F, et al. Particle laden fluid interfaces: dynamics and interfacial rheology. Adv Colloid Interface Sci 2014;206:303–19.
[9] Tcholakova S, Mitrinova Z, Golemanov K, Denkov ND, Vethamuthu M, Ananthapadmanabhan KP. Control of Ostwald ripening by using surfactants with high surface modulus. Langmuir 2011;27:14807–19.
[10] Cox AR, Aldred DL, Russell AB. Exceptional stability of food foams using class II hydrophobin HFBII. Food Hydrocoll 2009;23:366–76.
[11] Cox AR, Cagnol F, Russell AB, Izzard MJ. Surface properties of class II hydrophobins from Trichoderma reesei and influence on bubble stability. Langmuir 2007;23:7995–8002.
[12] Blijdenstein TBJ, de Groot PWN, Stoyanov SD. On the link between foam coarsening and surface rheology: why hydrophobins are so different. Soft Matter 2010;6:1799–808.
[13] Aumaitre E, Vella D, Cicuta P. On the measurement of the surface pressure in Langmuir films with finite shear elasticity. Soft Matter 2011;7:2530–7.
[14] Radulova GM, Golemanov K, Danov KD, Kralchevsky PA, Stoyanov SD, Arnaudov LN, et al. Surface shear rheology of adsorption layers from the protein HFBII hydrophobin: effect of added β-casein. Langmuir 2012;28:4168–77.
[15] Danov KD, Radulova GM, Kralchevsky PA, Golemanov K, Stoyanov SD. Surface shear rheology of hydrophobin adsorption layers: laws of viscoelastic behaviour with applications to long-term foam stability. Faraday Discuss 2012;158:195–221.
[16] Alexandrov NA, Marinova KG, Gurkov TD, Danov KD, Kralchevsky PA, Stoyanov SD, et al. Interfacial layers from the protein HFBII hydrophobin: dynamic surface tension, dilatational elasticity and relaxation times. J Colloid Interface Sci 2012;376:296–306.
[17] Russo PS, Blum FD, Ipsen JD, Abul-Hajj YJ, Miller WG. The surface activity of the phytotoxin cerato-ulmin. Can J Bot 1982;60:1414–22.
[18] Basheva ES, Kralchevsky PA, Christov NC, Danov KD, Stoyanov SD, Blijdenstein TBJ, et al. Unique properties of bubbles and foam films stabilized by HFBII hydrophobin. Langmuir 2011;27:2382–92.
[19] Blijdenstein TBJ, Ganzevles RA, de Groot PWN, Stoyanov SD. On the link between surface rheology and foam disproportionation in mixed hydrophobin HFBII and whey protein systems. Colloids Surf A 2013;438:13–20.
[20] Wang Y, Bouillon C, Cox A, Dickinson E, Durga K, Murray BS, et al. Interfacial study of class II hydrophobin and its mixtures with milk proteins: relationship to bubble stability. J Agric Food Chem 2013;61:1554–62.
[21] Burke J, Cox A, Petkov J, Murray BS. Interfacial rheology and stability of air bubbles stabilized by mixtures of hydrophobin and β-casein. Food Hydrocoll 2014;34:119–27.
[22] Reger M, Sekine T, Okamoto T, Hoffmann H. Unique emulsions based on biotechnically produced hydrophobins. Soft Matter 2011;7:8248–57.
[23] Reger M, Sekine T, Okamoto T, Watanabe K, Hoffmann H. Pickering emulsions stabilized by novel clay – hydrophobin synergism. Soft Matter 2011;7:11021–30.
[24] Reger M, Sekine T, Hoffmann H. Boosting the stability of protein emulsions by the synergistic use of proteins and clays. Colloid Polym Sci 2012;290:631–40.
[25] Marinova KG, Basheva ES, Nenova B, Temelska M, Mirarefi AY, Campbell B, et al. Physico-chemical factors controlling the foamability and foam stability of milk proteins: sodium caseinate and whey protein concentrates. Food Hydrocoll 2009;23:1864–76.
[26] Qin M, Wang L-K, Feng X-Z, Yang Y-L, Wang R, Wang C, et al. Bioactive surface modification of mica and poly(dimethylsiloxane) with hydrophobins for protein immobilization. Langmuir 2007;23:4465–71.
[27] Li X, Hou S, Feng X, Yu Y, Ma J, Li L. Patterning of neural stem cells on poly(lactic-co-glycolic acid) film modified by hydrophobin. Colloids Surf B 2009;74:370–4.
[28] Zhang XL, Penfold J, Thomas RK, Tucker IM, Petkov JT, Bent J, et al. Adsorption behavior of hydrophobin and hydrophobin/surfactant mixtures at the solid – solution interface. Langmuir 2011;27:10464–74.
[29] Basheva ES, Kralchevsky PA, Danov KD, Stoyanov SD, Blijdenstein TBJ, Pelan EG, et al. Self-assembled bilayers from the protein HFBII hydrophobin: nature of the adhesion energy. Langmuir 2011;27:4481–8.
[30] Stanimirova RD, Gurkov TD, Balashev KT, Kralchevsky PA, Stoyanov SD, Pelan EG. Surface pressure and elasticity of hydrophobin HFBII layers on the air – water interface: rheology vs. structure detected by AFM imaging. Langmuir 2013;29:6053–67.
[31] Linder MB. Hydrophobins: proteins that self assemble at interfaces. Curr Opin Colloid Interface Sci 2009;14:356–63.
[32] Petkov JT, Gurkov TD, Campbell BE, Borwankar RP. Dilatational and shear elasticity of gel-like protein layers on air/water interface. Langmuir 2000;16:3703–11.
[33] Erni P, Fischer P, Windhab EJ, Kusnezov V, Stettin H, Läuger J. Stress- and strain-controlled measurements of interfacial shear viscosity and viscoelasticity at liquid/liquid and gas/liquid interfaces. Rev Sci Instrum 2003;74:4916–24.
[34] Borbas R, Murray BS, Kiss E. Interfacial shear rheological behavior of proteins in three-phase partitioning systems. Colloids Surf A 2003;213:93–103.
[35] Scheludko A, Exerowa D. Instrument for interferometric measurements of the thickness of microscopic foam films. Commun Dept Chem Bulg Acad Sci 1959;7:123–32.
[36] Sheludko A. Thin liquid films. Adv Colloid Interface Sci 1967;1:391–464.
[37] Kralchevsky PA, Danov KD, Basheva ES. Hydration force due to the reduced screening of the electrostatic repulsion in few-nanometer-thick films. Curr Opin Colloid Interface Sci 2011;16:517–24.
[38] Wierenga PA, Basheva ES, Denkov ND. Modified capillary cell for foam film studies allowing exchange of the film-forming liquid. Langmuir 2009;25:6035–9.
[39] Mysels KJ, Jones MN. Direct measurement of the variation of double-layer repulsion with distance. Discuss Faraday Soc 1966;42:42–50.
[40] Exerowa D, Kolarov T, Khristov Khr. Direct measurement of disjoining pressure in black foam films. I. Films from an ionic surfactant. Colloids Surf 1987;22:161–9.
[41] Schelero N, Hedicke G, Linse P, von Klitzing R. Effects of counterions and co-ions on foam films stabilized by anionic dodecyl sulfate. J Phys Chem B 2010;114:15523–9.
[42] Dimitrova TD, Leal-Calderon F, Gurkov TD, Campbell B. Disjoining pressure vs thickness isotherms of thin emulsion films stabilized by proteins. Langmuir 2001;17:8069–77.
[43] Krägel J, Wüstneck R, Husband F, Wilde PJ, Makievski AV, Grigoriev DO, et al. Properties of mixed protein/surfactant adsorption layers. Colloids Surf B 1999;12:399–407.
[44] Hyun K, Wilhelm M, Klein CO, Cho KS, Nam JG, Ahn KH, et al. A review of nonlinear oscillatory shear tests: analysis and application of large amplitude oscillatory shear (LAOS). Prog Polym Sci 2011;36:1697–753.
[45] Acierno D, Mantia FP, Marrucci G, Titomanlio G. A non-linear viscoelastic model with structure-dependent relaxation times: I. Basic formulation. J Non-Newton Fluid Mech 1976;1:125–46.
[46] Acierno D, La Mantia FP, Marrucci G, Rizzo G, Titomanlio G. A non-linear viscoelastic model with structure-dependent relaxation times: II. Comparison with l.d. polyethylene transient stress results. J Non-Newton Fluid Mech 1976;1:147–57.
[47] Barnes HA. Thixotropy — a review. J Non-Newton Fluid Mech 1997;70:1–33.
[48] Panaiotov I, Dimitrov DS, Ter-Minassian-Saraga L. Dynamics of insoluble monolayers. II. Viscoelastic behavior and Marangoni effect for mixed protein phospholipid films. J Colloid Interface Sci 1979;72:49–53.
[49] Vassilev PM, Taneva S, Panaiotov I, Georgiev G. Dilatational viscoelastic properties of tubulin and mixed tubulin-lipid monolayers. J Colloid Interface Sci 1981;84:169–74.
[50] Panaiotov I, Tz Ivanova, Proust J, Boury F, Denizot B, Keough K, et al. Effect of hydrophobic protein SP-C on structure and dilatational properties of the model monolayers of pulmonary surfactant. Colloids Surf B 1996;6:243–60.
[51] Hambardzumyan A, Aguié-Béghin V, Panaiotov I, Douillard R. Effect of frequency and temperature on rheological properties of β-casein adsorption layers. Langmuir 2003;19:72–8.
[52] Ivanova Tz, Minkov I, Panaiotov I, Saulnier P, Proust JE. Dilatational properties and morphology of surface films spread from clinically used lung surfactants. Colloid Polym Sci 2004;282:1258–67.
[53] Adams JJ, Anderson BF, Norris GE, Creamer LK, Jameson GVB. Structure of bovine β-lactoglobulin (variant A) at very low ionic strength. J Struct Biol 2006;154:246–54.
[54] Popa I, Gillies G, Papastavrou G, Borkovec M. Attractive electrostatic forces between identical colloidal particles induced by adsorbed polyelectrolytes. J Phys Chem B 2009;113:8458–61.
[55] Majhi PR, Ganta RR, Vanam RP, Seyrek E, Giger K, Dubin PL. Electrostatically driven protein aggregation: β-lactoglobulin at low ionic strength. Langmuir 2006;22:9150–9.
[56] Farrell Jr HM, Wickham ED, Unruh JJ, Qi PX, Hoagland PD. Secondary structural studies of bovine caseins: temperature dependence of β-casein structure as analyzed by circular dichroism and FTIR spectroscopy and correlation with micellization. Food Hydrocoll 2001;15:341–54.
[57] Horne DS. Casein micelle structure: models and muddles. Curr Opin Colloid Interface Sci 2006;11:148–53.
[58] Portnaya I, Cogan U, Livney YD, Ramon O, Shimoni K, Rosenberg M, et al. Micellization of bovine β-casein studied by isothermal titration microcalorimetry and cryogenic transmission electron microscopy. J Agric Food Chem 2006;54:5555–61.

[59] Graham DE, Phillips MC. Proteins at liquid interfaces III. Molecular structures of adsorbed films. J Colloid Interface Sci 1979;70:427–39.
[60] Noskov BA, Latnikova AV, Lin S-Y, Loglio G, Miller R. Dynamic surface elasticity of β-casein solutions during adsorption. J Phys Chem C 2007;111:16895–901.
[61] Marinova KG, Stanimirova RD, Georgiev MT, Alexandrov NA, Basheva ES, Kralchevsky PA. Co-adsorption of the proteins β-casein and BSA in relation to the stability of thin liquid films and foams. In: Kralchevsky PA, Miller R, Ravera F, editors. Colloid and interface chemistry for nanotechnology. Boca Raton, FL: CRC Press; 2013. p. 439–58 (http://www.crcnetbase.com/doi/abs/10.1201/b15262-22).
[62] Stubenrauch C, Rojas OJ, Schlarmann J, Claesson PM. Interactions between nonpolar surfaces coated with the nonionic surfactant hexaoxyethylene dodecyl ether $C_{12}E_6$ and the origin of surface charges at the air/water interface. Langmuir 2004;20:4977–88.